

New airfoils for microhorizontal-axis wind turbines

Manoj Kumar Chaudhary* and S. Prakash

Department of Mechanical Engineering, Sathyabama Institute of Science and Technology, Chennai, Tamil Nadu, India.

* Corresponding Author: manojz2011@gmail.com

Submitted : 29/06/2020

Revised : 25/12/2020

Accepted : 16/03/2021

ABSTRACT

In this study, small horizontal-axis wind turbine blades operating at low wind speeds were optimized. An optimized blade design method based on blade element momentum (BEM) theory was used. The rotor radius of 0.2 m, 0.4 m, and 0.6 m and blade geometry with single (W1 & W2) and multistage rotor (W3) were examined. MATLAB and XFOIL programs were used to implement to BEM theory and devise a six novel airfoil (NAF-Series) suitable for application of small horizontal axis wind turbines at low Reynolds number. The experimental blades were developed using the 3D printing additive manufacturing technique. The new airfoils such as NAF3929, NAF4420, NAF4423, NAF4923, NAF4924, and NAF5024 were investigated using XFOIL software at Reynolds numbers of 100,000. The investigation range included tip speed ratios from 3 to 10 and angle of attacks from 2° to 20°. These parameters were varied in MATLAB and XFOIL software for optimization and investigation of the power coefficient, lift coefficient, drag coefficient, and lift-to-drag ratio. The cut-in wind velocity of the single and multistage rotors was approximately 2.5 and 3 m/s, respectively. The optimized tip speed ratio, axial displacement, and angle of attack were 5.5, 0.08m, and 6°, respectively. The proposed NAF-Series airfoil blades exhibited higher aerodynamic performances and maximum output power than those with the base SG6043 and NACA4415 airfoils at low Reynolds number.

Keywords: Blade geometry; 3D printer; Power coefficient; Solidity; Tip speed ratio.

INTRODUCTION

Energy is the foundation for economic and social development. Wind is a renewable energy source used by wind turbines to generate electricity. The small horizontal-axis wind turbine requires a minimum wind speed of 4.2 m/s using an optimized blade, which could reduce the starting rotor speed without external force allowing it to be used in roadside or housetop applications (Lee *et al.*, 2016; Ismail *et al.*, 2018; & Abrar *et al.*, 2014). The torque-producing power was obtained mainly from the tip region of the turbine blade (Wright and Wood, 2004; Clifton and Wood, 2007). The Blade Element Momentum (BEM) model offers excellent accuracy and high computational efficiency for the blade design calculation of propeller performance. The maximum power coefficient value of 0.371 for the rotor tested and 0.388 for the optimized rotor is achieved at wind speed of 6 m/s approximately (Gur and Rosen, 2008; Hassanzadeh *et al.*, 2016). Blade element momentum (BEM) and computational fluid dynamics (CFD) were analyzed from three different turbulence models. For rural applications, a 2-kW small horizontal axis wind

turbine with a rotor radius of 1.8 m and a tip speed ratio (TSR) of 6 at low wind speed was examined (Chaudhary and Prakash, 2019; Suresh and Rajakumar, 2019). Rosenberg *et al.*, 2014, proposed and investigated a dual-rotor turbine design. A smaller, aerodynamically tailored, secondary coaxial rotor is mounted ahead of the main rotor in this dual rotor concept. Nugroho *et al.*, 2019, studied the multistage wind turbine which was better than the single rotor at the same tip speed ratio, and optimum (X/D) axial distance ratio is 0.18. Sustainable development is one of the main objectives of future planning. It corresponds energetically to higher energy efficiency and the use of renewable energy sources. The manufacturing method required a rapid prototype of the various iterations of blade designs (Poole and Phillips, 2015; Duquette and Visser, 2003; Singh and Ahamed, 2013). The main objectives of this present study are to create and investigate the novel airfoil for small wind turbine with single and multistage rotors at low Reynolds numbers. For the experimental investigations in this research, the wind tunnel experiments were performed to measure the power of 3 & 6 bladed rotor blades at various wind speeds and blade pitch angles. The rotor blade material used is acrylonitrile butadiene styrene (ABS) and polylactic acid (PLA) fabricated by using the fused deposition method (FDM). The main objectives of this paper can be listed as follows.

- Investigation of the aerodynamic performance and development of new airfoil of NAF3929, NAF4420, NAF4423, NAF4923, NAF4924, and NAF5024 designed for small wind turbines at low Reynolds number.
- Experimental & numerical investigation of small HAWT blades for single and multistage rotors for different airfoils, axial displacement with different solidity.
- Obtaining of the small wind turbine parameters, output power, blade pitch angle, power coefficient, blade geometry, and solidity for various wind turbine models.
- Optimization of the geometrical dimensions of the NAF4923 airfoil to increase the wind turbine performance.

AIRFOIL AND BLADE DESIGN METHODOLOGY

The investigations and development of airfoils are based on the thickness to camber ratios. The XFOIL has been used in the selection of airfoil processes to simulate and analyze a number of existing Low-Re HAWT airfoils. The SG6043 and NACA4415 airfoils were selected from literature and XFOIL results for comparisons of aerodynamic performances of new airfoils. The new airfoil is designated as NAF. In this work, airfoils were designed and optimized such as NAF3929, NAF4420, NAF4423, NAF4923, NAF4924, and NAF5024 for application of small horizontal axis wind turbine rotors. Jayapriya *et al.*, 2019, studied the multirotor design that can be used to increase power generation at locations where space is small.

Airfoil is one of the most important parameters of the rotor blade design and development. In order to enhance the power coefficient and torque generated, the lift-to-drag ratio for the airfoil must be amplified (Chaudhary and Roy, 2015; Singh and Ahmed, 2012). The 251 panels were considered for analysis of aerodynamic characteristics of airfoils by using XFOIL software as depicted in Fig. 1. The geometric shapes of the new airfoil showed significant changes, the thickness-chamber ratios and the leading edge radius. The Reynolds number and the N_{crit} were independently modified, by combinations of the maximum lift coefficient and the lift-drag ratios. The aerodynamic performance of six new airfoils geometries was compared as existing low Re airfoils. SG6043 and NAF4923 airfoils exhibited an outstanding CL/CD ratio which is necessary to maximize the power output. SG6043 has a maximum thickness of 10%, which may cause high stress levels near the root. The new airfoil NAF4923 had a thickness of 12.80%, with the maximum thickness position of 29.70%, maximum camber of 5.71%, with the maximum camber position of 41.90% relative to the chord length. The lift coefficients of the new airfoil (NAF series) are larger than those of the NACA4415 and SG6043 airfoils. The new airfoil achieved a maximum CL/CD ratio at angle of attack = 5° to 6°, whereas the SG6043 airfoil achieved a maximum CL/CD at an angle of attack between 6° and 7°. However, NACA4415 airfoil, the maximum CL/CD ratio was obtained approximately at α of 7° for a Reynolds number of 1×10^5 . The 3 different blade models with rotor radius of 0.2 m, 0.4 m, and 0.6 m with different rotor solidity,

respectively, were investigated and presented in Tab. 1. The design of rotor blade & the airfoil with optimum axial distance between two rotors are illustrated in Fig. 2 & Fig. 3. The optimum axial distance ratio is 0.18 (Nugroho et al., 2019).

Table 1. Wind turbine blade specification.

Rotor type	Rotor radius (m)	Solidity	Airfoil
R1	0.2	0.1181	NAF4923
R2	0.4	0.1463	NAF4923
R3	0.6	0.0523	NAF4923

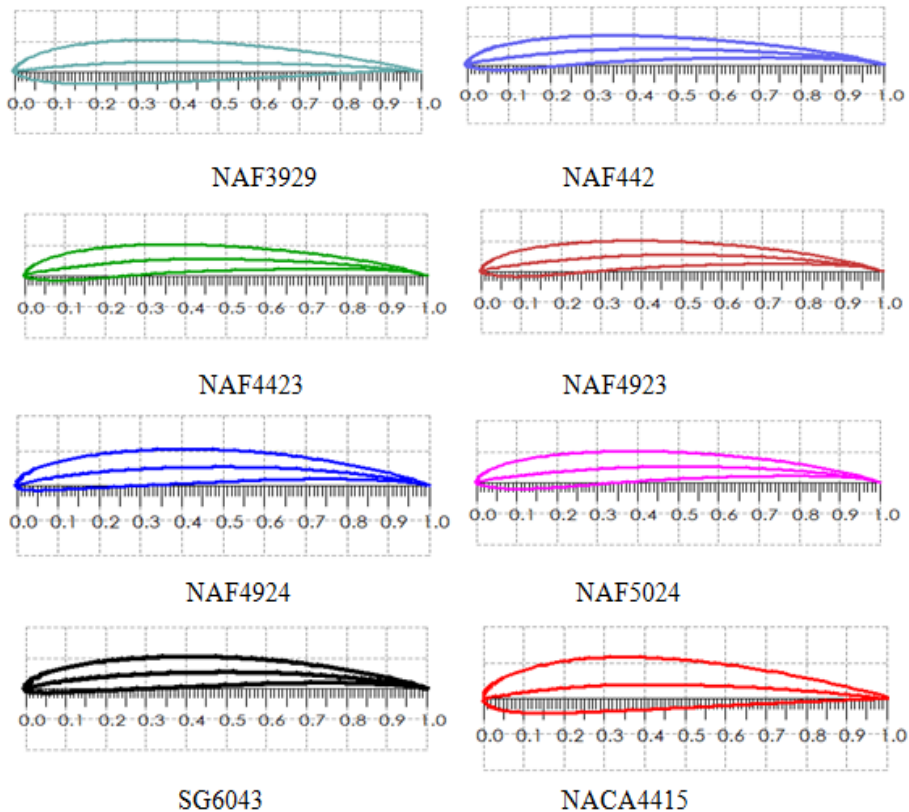


Figure 1. Airfoils generation in XFOIL software: NAF3923, NAF4420, NAF4423, NAF4923, NAF4924, NAF5024, NACA4415, and SG6043.

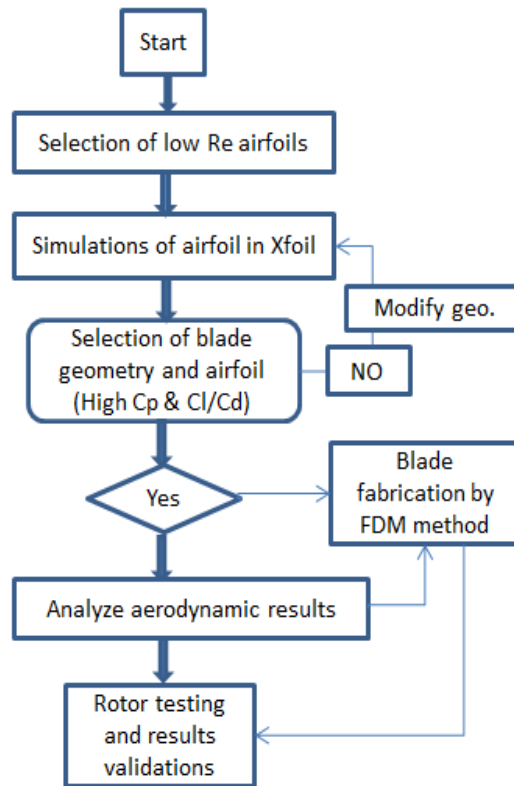


Figure 2. Flow chart of the methodology used for airfoil selection, blade design, and rotor testing.

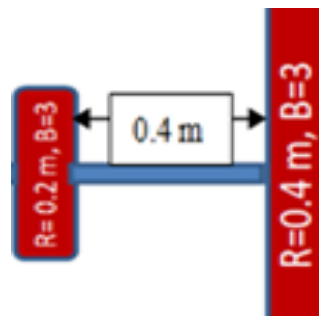


Figure 3. Rotor configuration.

MODELING AND ANALYSIS

The small wind turbine blade for a rotor with solidity of 11.81%, 14.63%, and 5.23% which was manufactured using the ABS and PLA material, with FDM method, was studied for optimization and experimentations at different blade pitch angles that are presented in Tab. 1. The selection of rotor radius with respect to wind speed at Reynolds number of 100,000 is illustrated in Fig. 4. The optimized blade geometry of rotors R1, R2, and R3 is shown in Fig. 5. The variations of the twist angle with sectional blade length at $\lambda = 6$ for new airfoil B = 3 are presented in Fig. 6, for rapid prototype fabrications. The R1, R2, and R3 of Xfoil and 3D printed optimization blade models are shown

in Fig. 7. The R2 blades were designed for higher solidity; however, the R3 model was optimized at lower solidity. The rotor performance was investigated using XFOil. The optimization of 3D printed W1 and W2 fabricated with FDM method was shown in Fig. 7. The single-stage rotor was designated as W1 and W2. However, W3 rotor designated for multistage wind turbine rotor. The rotor arrangement for experimentations is depicted in Tab. 2. The calculation procedure enables calculating the optimum blade geometry of small wind turbine, including its aerodynamic performance [Ismail *et al.*, 2018; Chaudhary and Roy, 2015].

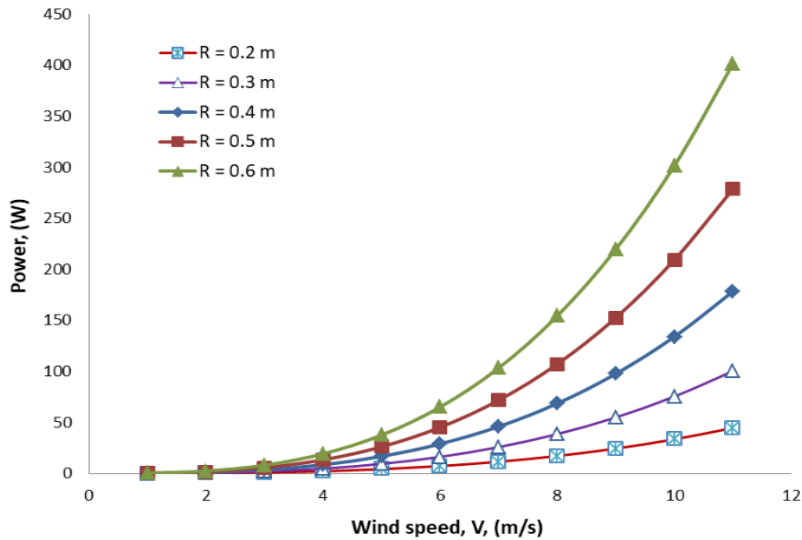


Figure 4. Selections of rotor radius.

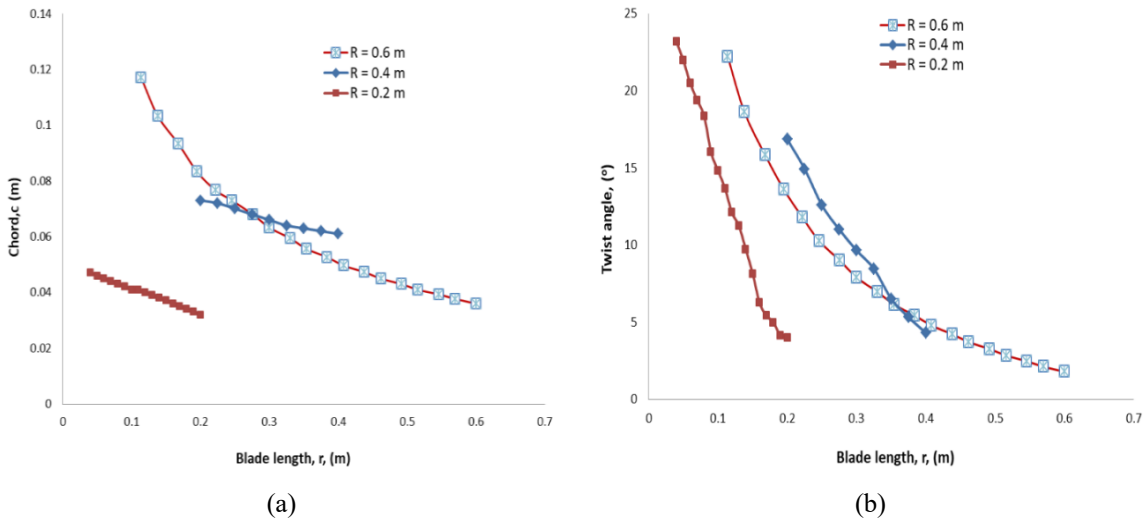


Figure 5. Optimum blade geometry of 0.2m, 0.4m, and 0.6m rotor radius. (a) Chord distribution along the blade length. (b) Blade twist distribution along the blade length.

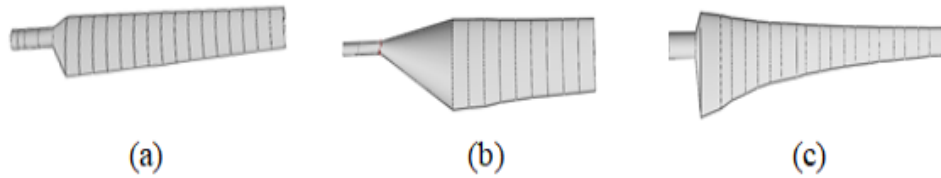


Figure 6. Optimum blade models: (a) R1, (b) R2, and (c) R3.

Table 2. Rotors configuration for experimentations.

Blade types	Rotor types	Rotor radius (m)	Number of blades	Material
R1	W1	0.2	3	ABS
R2	W2	0.4	3	PLA
R1 & R2	W3	$R_f = 0.2$ & $R_r = 0.4$	6	ABS & PLA

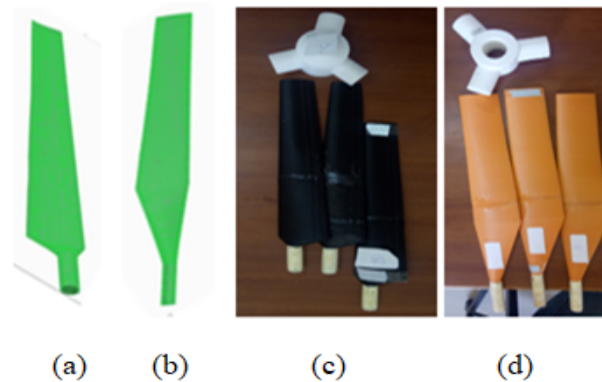


Figure 7. Three-dimensional geometry of blade models (a-b) R1 & R2 blade optimized in Cura software (c-d) 3D printed blade models of R1 & R2.

EXPERIMENTATIONS

The small wind turbine blade geometries and design parameters are presented in Tab. 3. The new airfoil model created in XFOIL software was shown in Fig. 8. The airfoil model and rotor blade are fabricated by wooden, printing ABS, and PLA filaments materials, respectively, as shown in Fig. 9. The Creo models were transformed from the format into G code using Cura software and imported to the 3D printer. The printer was run under the following conditions: printing resolution was set to 0.001 m, nozzle temperature was adjusted to 205°C, bed temperature was 60°C, and the printing speed was tuned to 50 mm/s. The fabrication of the blade by using the new NAF4923 airfoil is illustrated in Fig. 7. The experiments were conducted in an open wind tunnel in the fluid mechanics laboratory at the Dr. D. Y. Patil School Engineering India affiliated to the SPPU University. Fig. 10 (a-b) & Fig. 11 (a) show the tests stands used in the fabrication and experiment for wind turbine blades. The wind tunnel has a test section of 0.3 m × 0.3 m × 1 m. Technical instrumentation specifications are shown in Tab. 4. The experimental tests have been

conducted to determine output power of rotor (W3) at axial displacement of 0.04m, 0.06m, & 0.08m at different wind speeds in wind tunnel.

Table 3. Design parameters simulation details.

Parameters	Descriptions
Base airfoil selection	SG6043 & NACA4415
Angle of attack (α)	2° to 20°
Tip speed ratio (λ)	2 to 8
Solidity (σ)	0.0523 to 0.1463
New airfoil series	NAF
Reynolds No.	100000
Rotor radius	0.2 m, 0.4m, & 0.6m



Figure 8. Airfoil model created in Xfoil.

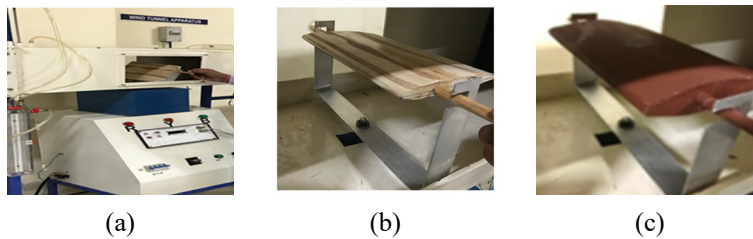


Figure 9. Experimental setup. (a) Controller unit, (b) 3D printer, and (c) wind tunnel.

Table 4. Test instrument details for experimentations.

Instrument	Model number	Measurement range	Resolutions	Temperature range
Anemometer	AVM-06	0.5–30 m/s	0.1 m/s	0 – 60 °C
Tachometer	HTM-560	10 to 1000 rpm	0.1 rpm	0 – 60 °C
Multimeter	AVF-19N	0.2 – 230 V	0.1 volt	0 – 60 °C
Wind tunnel	WT-02	1 -30 m/s	1 m/s	0 – 60 °C

From 0.075 to 0.3 m, the operating temperature ranges from 0 to 60 °C. In this work, the coaxial series rotors wind turbines with two rotors are considered as shown in Fig. 11(b). Fig. 12 shows the setup of inverter battery system. The decrease in wind speed causes the torque generated by the second rotor increases from torque generated by the first rotor to compensate for the rotation of the first rotor. High torque increases mechanical power generated by the second rotor at lower wind power.



Figure 10. Experimental setup. (a) 3D printer. (b) Wind tunnel.

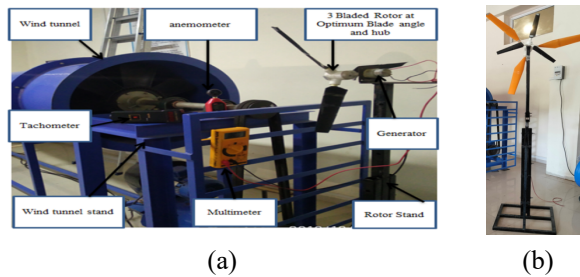


Figure 11. Schematic layout of the experimentations pictures: (a) W1, (b) W2, & W3

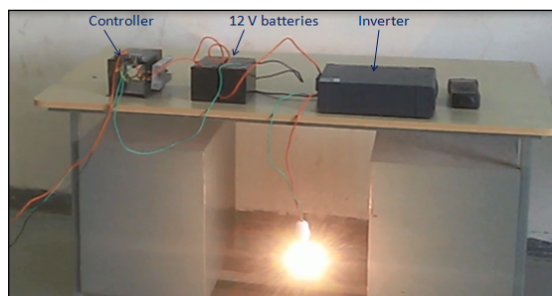


Figure 12. Inverter battery setup.

RESULTS AND DISCUSSIONS

The results of the numerical and experimental investigations for all cases are presented in this section. Experimental cases of single & multistage wind turbine rotor with wind velocity from the cut-in speed (2.5 to 3 m/s) to the rated wind speed (8 m/s) and the configurations of the rotor blade pitch angles vary from 0° to 90°. The MATLAB code of blade design is provided in A1 (Appendix).

AIRFOIL EFFECTS ON ROTOR PERFORMANCES

The NAF-Series airfoil was compared with SG6043 and NACA4415 base airfoils for low Reynolds number application for small horizontal axis wind turbines. The new airfoils were designed and tested with XFOil at $Re = 100000$. The AF300 airfoil was optimized from existing low Reynolds number airfoils using XFOil software (Singh *et al.*, 2012). For each airfoil, the polar curves were obtained for angle of attack, α , varying from 0° to 20° to satisfy all velocity conditions of the investigated airfoils. Figs 13(a-b) show the graphs of lift and lift-to-drag ratio for the 8 airfoil at $Re=100000$. From Fig 13(a), it was observed that the lift coefficient values are strongly influenced by the angle of attack (α). From the results in the graph it can be observed that NAF-Series airfoil has highest lift coefficient values in the angle of attack ranges of 8° - 12° . From the results in the graph, it can be observed that NAF4420 and SG6043 airfoils produce maximum C_L of 1.6 and 1.65 at angle of attack, α , of 12° & 14° , respectively. NAF4924 airfoil produces maximum C_L of 1.5 at α of 16° . After 12° angle of attack, the value of C_L for NAF airfoil decreases up to angle of attack, $\alpha = 16^\circ$ except NAF4924 airfoil, and beyond 16° angle of attack, the value of $C_L = 1.35 - 1.5$ remains constant up to 20° angle of attack. Airfoils NAF3929, NAF 4420, NAF4423, NAF4923, NAF4924, NAF5024, SG6043, and NACA4415 had maximum C_L of 1.35, 1.6, 1.5, 1.55, 1.5, 1.5, 1.65, and 1.48 at angle of attack, α , of 12° - 16° . The airfoils NAF4923, NAF4924, and SG6043 showed soft stall behaviour in the angle of attack range of 12° - 16° . The maximum value of the lift-drag ratio for the new airfoil was observed at an angle of attack of 5° - 6° at $Re = 100,000$ except NAF3929.

The NAF3929, SG6043, and NACA4415 have maximum lift-to-drag ratio at angle of attack 8° , 7° , and 10° , respectively. The lift coefficient of the NAF4923 airfoil was 10-15 % higher than that for the SG6043 airfoil because of the large camber and thickness, as depicted in Figs. 13 (a-b), at the angle of attack 2° - 10° . The high lift coefficient and its high AOA, α , at low speeds facilitated the rotor start up and enhanced its performance at low wind velocities, thus providing adequate characteristics when used in small power rotors. Fig 13(b) shows the variation of lift-to-drag ratio (C_L/C_D) for different airfoils at a Low Reynolds number $=100,000$. Maximum lift-to-drag ratios (C_L/C_D) of 69 were produced by NAF4923 and NAF4924 airfoil at α of 6° & 5° , respectively, followed by SG6043 and NACA4415 airfoils of 66 and 48 at α of 7° & 10° , respectively. Airfoils NAF3929, NAF4420, NAF4423, and NAF5024 have maximum lift-to-drag ratio (C_L/C_D) = 49, 66, 66.5, and 68, respectively, at $\alpha = 8^\circ$, 5° , 6° , and 6° , respectively. The NAF4923 and SG6043 airfoils produced lowest values of C_L/C_D ratios of 40 and 35 at angle of attack, $\alpha = 2^\circ$, respectively. Finally, from the obtained results of XFOil, it was found that the NAF4923, NAF4924, and SG6043 airfoils had their peak values of lift-to-drag ratios producing at particular α value, while NAF5024 and NACA4415 airfoils have a wide range of C_L/C_D ratios and showed a soft stall behavior in the angle of attack, α , with the range of 2° - 10° . It was seen that the NAF-Series airfoil is the best profile for small horizontal axis wind turbines at low Reynolds number application. The maximum value of the C_L/C_D ratio for the designed and optimized airfoil was observed at an AOA (angle of attack) of 5° to 6° at Reynolds number $=100,000$. We had investigated the effect of the airfoil section on the aerodynamic performance of the various small wind turbine rotors. The proposed airfoil was thicker than the SG6043 airfoil. Fig. 14 indicates the influence of airfoil on the blade performances. As it can be seen the maximum power coefficient is obtained by NAF4923 and SG6043 at $\lambda = 5$. The BEMT-based design program was developed for tip speed ratios ranging from 2 to 8. The C_p - λ curve was obtained using XFOil software.

The solidities of 5.23 % with variable chord and twisted blade geometry were analyzed at $Re=100,000$ of NAF4923 and SG6043 with and without root-tip losses for blade numbers, $B=3$, and the results are illustrated in Fig 14. From Fig. 14, maximum power coefficient of R3 blade model had 0.515 and 0.46 for without and with root-tip losses at $\lambda = 5$. The values of λ increase from 5, and the values of power coefficient of SG6043 airfoil decrease as compared to the NAF4923 airfoil. Hence, we have selected novel airfoil NAF4923 for blade fabrications and experimentations. The variation of output power of R1 rotor is shown in Fig. 15. The optimum blade pitch angles are 30° of the rotor R1.

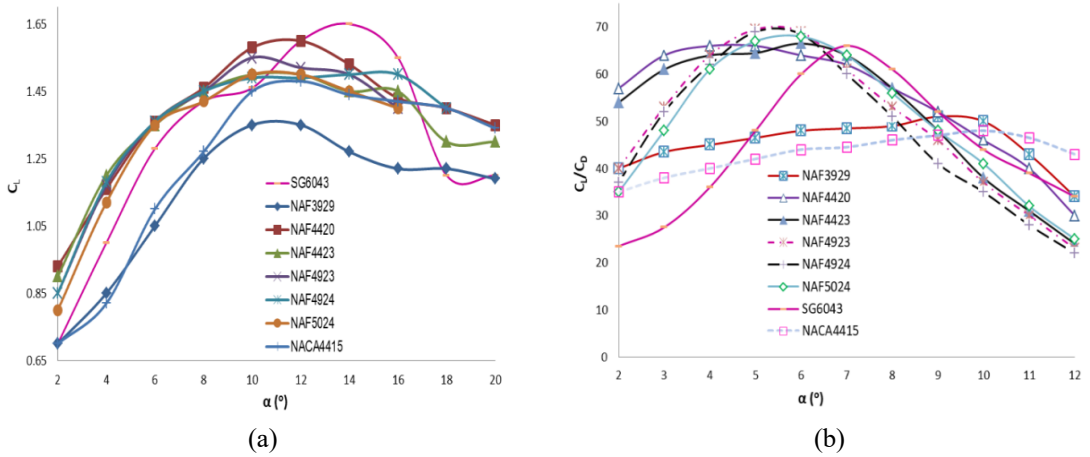


Figure 13. Variations of aerodynamic performances of different airfoils: (a) C_L vs α and (b) C_L/C_D vs α .

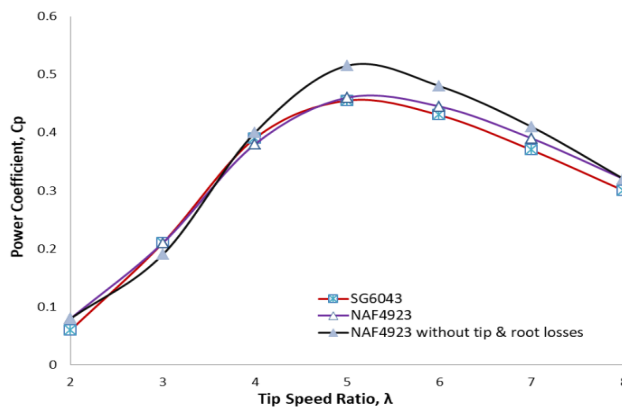


Figure 14. Variations of power coefficient of NAF4923 and SG6043 airfoils of R3 blade model with and without blade root and tip losses.

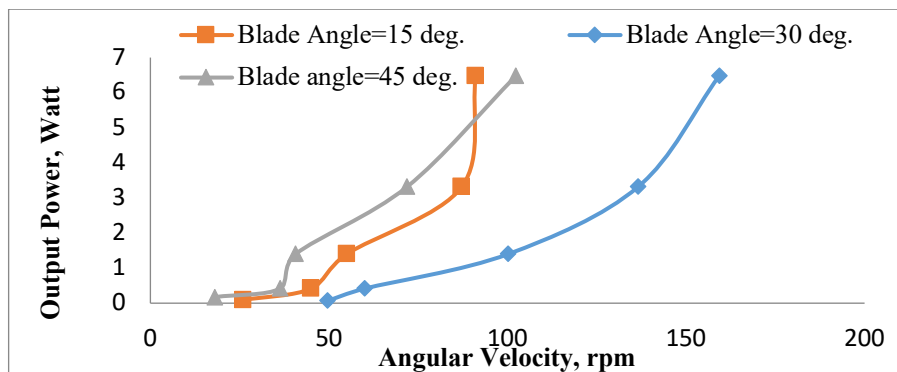


Figure 15. Variation of output power versus angular velocity of R1 rotor with optimum axial displacement of 0.08m at different blade pitch angles: (a) 15°, (b) 30°, and (c) 45°.

SOLIDITY EFFECT ON ROTOR PERFORMANCES

The solidity is one of the most important factor which greatly affects the performance of the horizontal axis wind turbine (HAWT). Fig. 16 indicates the influence of rotor solidity on the blade performances and tip speed ratios. It can be observed that the C_p values increase with a maximum tip speed ratio up to 4 for rotors R1 and R2 with solidity = 11.81% and 14.63%, respectively, and then they decrease. Moreover, the R3 blade model had maximum value of C_p obtained at $\lambda=5.5$. The main effect is to observe the changing solidity with respect to tip speed ratios as shown in Fig. 16. The maximum C_p had been obtained: R1, R2, and R3 of 0.36, 0.37, and 0.455 at tip speed ratios of 4, 4, and 5.5, respectively.

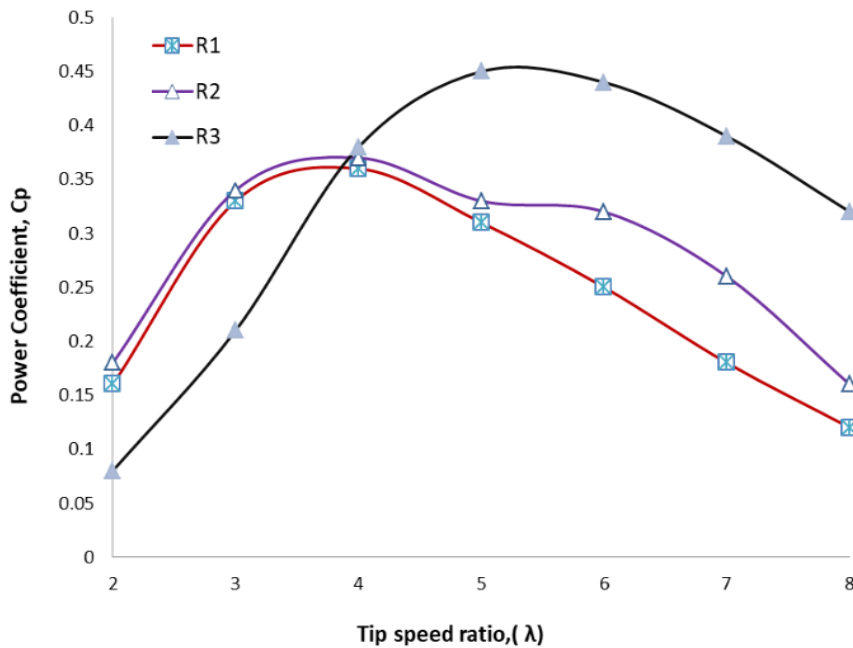


Figure 16. Power coefficient versus tip speed ratio at $Re=100,000$ for different rotors.

BLADE PITCH ANGLE AND ROTOR CONFIGURATIONS

The 3 wind turbine models were tested with the help of wind tunnel and blade pitch angles between 0° and 90° with increments of 15° . The rotational speeds were zero at the blade pitch angles of 0° and 90° . The rotors specifications are provided in Tab. 2. Figs. 17 (a-c) illustrate that experimentations results of rotor testing at optimization blade pitch angles of 15° , 30° , and 45° for 3 blades of single and multistage rotors. Figure 17 displays the variation of output power with different wind velocity at optimum blade pitch angles. The W1, W2, and W3 models were investigated and blade pitch angle of each rotor was optimized.

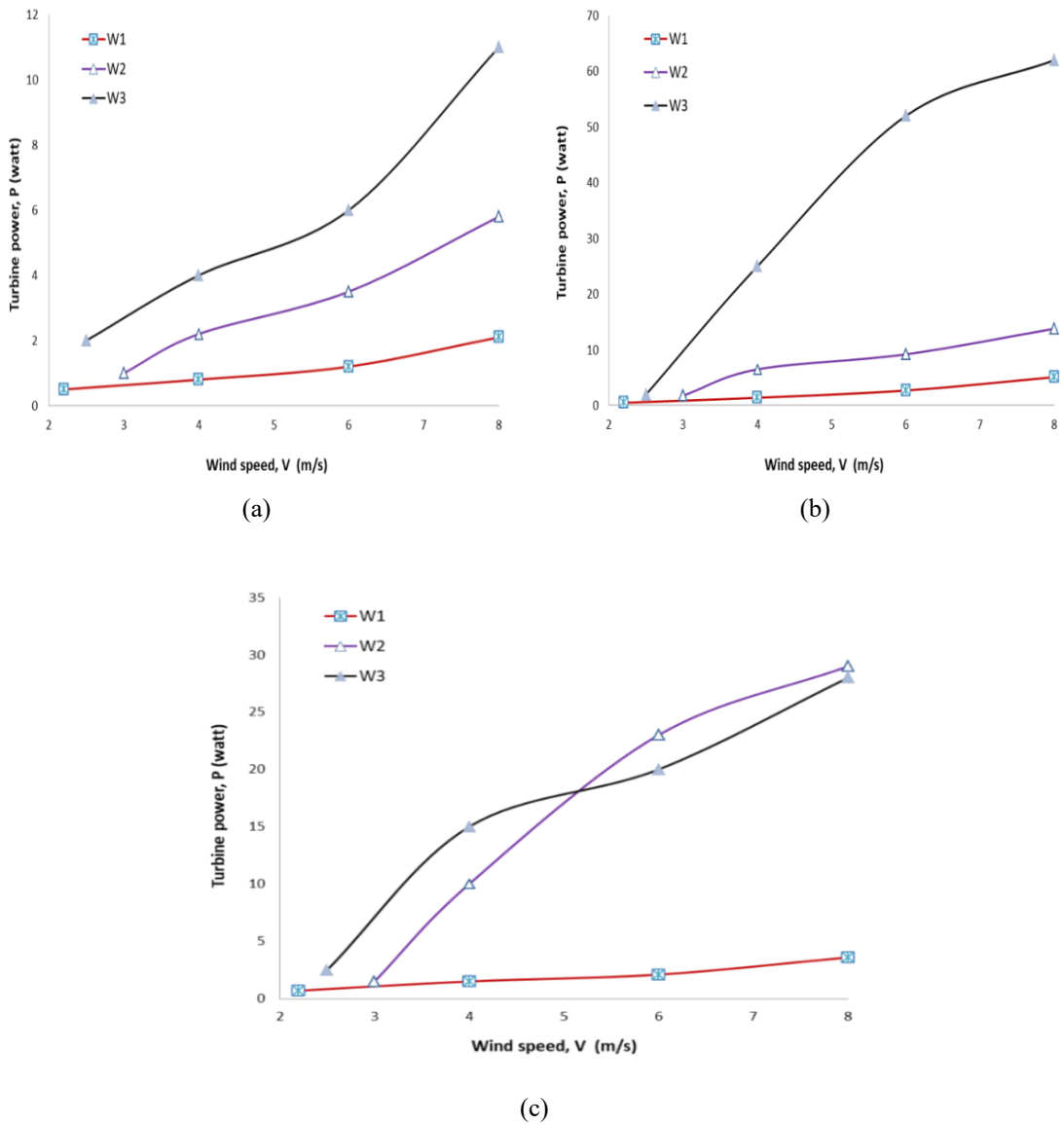


Figure 17. Power output of the different rotors at different wind speeds and blade pitch angles (a) 15°, (b) 30°, and (c) 45°.

The proposed airfoil NAF4923 and W3 rotor were most suitable as compared with W1 and W2 rotor. Rapid prototyping has considerable potential in manufacturing small blades because it does not require expensive molds and can produce blades for specific requirements. The starting wind velocity was 2 m/s of W1 rotors. However, the W2 and W3 models had cut-in wind speed of approximately 2.5 m/s. The optimization blade pitch angle of wind turbine rotors W1, W2, and W3 were at 30°, 45°, and 30°, respectively. The difference in mechanical power generated is affected by the axial displacement of the two rotors. The axial displacement of the two rotors affects the value of the wind speed that will hit the second rotor. In this research work, the axial displacement ratios between two rotors were selected as 0.08 m for W3 model. The optimization blade pitch angles for front (R_f) and rear (R_r) rotor were 30° & 45°, respectively. The results in the graph show maximum power produced by multistage wind turbine model (W3), at blade pitch angle of 30°. In W3 wind turbine model, the front and rear rotor radii were 0.2 m and 0.4 m, respectively.

The rotor W1 produces mechanical power = 2.1 W, 5.8 W, and 11 W at blade pitch angle of 15°, 30°, and 45° with rated wind speed = 8 m/s, respectively. Moreover, the rotor W2 produces mechanical power = 5.1 W, 13.8 W, and 62 W. Similarly, rotor W3 produces mechanical power = 3.6 W, 62 W, and 28 W at blade pitch angle of 15°, 30°, and 45° with rated wind speed = 8 m/s, respectively.

CONCLUSION

In this research work, the designed and creations of six new airfoils (NAF-Series) were tested in Xfoil at low Reynolds number. The numerical and experimental results indicated that NAF4923 was the most appropriate airfoil to obtain the maximum power coefficient as compared to the SG6043 airfoil. Six new airfoils were measured to analyze and compare C_L , C_L/C_D , with SG6043 and NACA4415 airfoils. The NAF-Series airfoil and blade geometry optimization are suitable for the design and development of small horizontal axis wind turbine rotors at low wind speed applications. Airfoils NAF3929, NAF4420, NAF4423, NAF4923, NAF4924, NAF5024, SG6043, and NACA4415 had maximum C_L of 1.35, 1.6, 1.5, 1.55, 1.5, 1.5, 1.65, and 1.48, respectively, at angle of attack, α , of 12°–16° at $Re = 100,000$. Airfoils NAF3929, NAF 4420, NAF4423, NAF4923, NAF4924, NAF5024, SG6043, and NACA4415 had maximum C_L/C_D of 49, 66, 66.5, 68, 69, 69, 66, and 48 at $\alpha = 8^\circ, 5^\circ, 6^\circ, 6^\circ, 5^\circ, 6^\circ, 7^\circ, \text{ and } 10^\circ$, respectively at $Re = 100,000$. The blade geometries of the NAF4923 and SG6043 were optimized based on BEMT with MATLAB and Xfoil. The rotor solidity equal to 11.81 %, 14.63 %, and 5.23 % of variable chord and twisted blade geometry were optimized and investigated with Xfoil. The maximum C_p had been obtained for blade models R1, R2, and R3 of 0.36, 0.37, and 0.455 at tip speed ratios, λ , of 4, 4, and 5.5, respectively. Three rotors were manufactured using NAF4923 airfoil section using the FDM method with low cost and less time. The three wind turbine models (W1, W2, and W3) were tested at different wind speeds, axial displacement, and blade pitch angles. From C_p - λ performance, W3 with axial distance between two rotors was 0.08 m, being capable of producing better performance as compared to rotors W1 and W2 at the rated wind speed of 8 m/s. The maximum multistage wind turbine (W3) performances at axial displacement of 0.08m. The NAF-Series airfoil is likely to be adopted for single and multistage horizontal axis wind turbines at low Reynolds number. The maximum power is produced by the rotor with solidity of 5.23 % at tip speed ratio of 5.5. The optimum blade pitch angles = 30°, 45°, and 30° for W1, W2, and W3 rotors, respectively. The maximum mechanical power was achieved by W3 rotor. It can be said that W3 type of multistage wind turbine can be utilized for electricity generations.

ACKNOWLEDGMENT

The authors thank Dr. D. Y. Patil School of Engineering for their support and providing the wind tunnel and FDM machines.

REFERENCES

- Abrar, M. A., Mahbub, A. M. & Mamun, M. 2014.** Design Optimization of a Horizontal Axis Micro Wind Turbine through Development of CFD Model and Experimentation, 10th International Conference on Mechanical Engineering Procedia, Engineering, **90**: 333-338.
- Chaudhary, M. K. & Roy, A. 2015.** Design & optimization of a small wind turbine blade for operation at low wind speed, World journal of Engineering. **12** (1); 83-94.
- Clifton-Smith, M.J. & Wood, D. H. 2007.** Further dual purpose evolutionary optimization of small wind turbine blades, J. Phys. Conf. Ser., **75**: 012017
- Chaudhary, M. K. & Prakash, S. 2019.** Investigation of Blade Geometry and Airfoil for Small Wind Turbine Blade Advanced Science, Engg and Medicine. **11** (5): 448-452.

- Duquette, M.M. & Visser, K. D. 2003.** Numerical Implication of Solidity and Blade Number on Rotor Performance of Horizontal-Axis Wind Turbines, *Journal of Solar Energy Engineering*. **125** (4):425-432.
- Gur, O. & Rosen, A. 2008.** Comparison between blade-element models of propellers. *Aeronaut J.* **112**:689–704
- Hassanzadeh, A., Hassanabad, H.H. & Dadvand, A. 2016.** Aerodynamic shape optimization and analysis of small wind turbine blades employing the Viterna approach for post-stall region, *Alexandria Engineering Journal*. **55** (3): 2035-2043.
- Ismail, A.R.K., Thiago, Canale. & Fatima, A.M. Lino. 2018.** Parametric analysis of Joukowski airfoil for 10-kW horizontal axis windmill, *Journal of the Brazilian Society of Mech. Sciences and Engineering*. **40**, Article no: 179.
- Jayapriya, J., Muruganandam, D., Raguraman, D., Senthilkumar, B., and Dhinakaran, V. 2019.** Design and Fabrication of Multi-Rotor Horizontal Axis Wind Turbine” *International Journal of Engineering and Advanced Technology (IJEAT)*, **8**(6):3500-3504.
- Lee, M.H., Shiah, Y.C. & Chi Jeng, B. 2016.** Experiments and numerical simulations of the rotor- blade performance for a small-scale horizontal axis wind turbine, *J. Wind Eng. Ind. Aerodynamics*. **149**: 17 – 29
- Nugroho, S., Diana, L. & Ariyanti, D. P. 2019.** Multistage Wind Turbine Capability to the Rotor Axial Distance Changes, *International Electronics Symposium (IES)*, Surabaya, Indonesia, 359-363.
- Poole, S. & Phillips, R. 2015.** Rapid Prototyping of Small Wind Turbine Blades Using Additive Manufacturing, *IEEE: South Africa*.
- Rosenberg, A., Selvaraj, S. & Sharma, A. 2014.** A novel dual-rotor turbine for increased wind energy capture. *Journal of Physics (TORQUE 2014)*, **524**:012078.
- Suresh, A. & Rajakumar, S. 2019.** Design of small horizontal axis wind turbine for low wind speed rural application, *Material today proceeding*. **23** (1):16-22
- Singh, R.K. & Ahamed, M.R. 2013.** Blade Design and Performance Testing of a Small Wind Turbine Rotor For Low Wind Speed Application, *Renewable Energy*. **50**:812-819.
- Singh, R.K., Ahmed, M.R., Zullah, M.A., & Lee, Y.H. 2012.** Design of a low Reynolds number airfoil for small horizontal axis wind turbines, *Renewable Energy*. **42**:66–76.
- Wright, A.K. & Wood, D.H. 2004.** The starting and low wind speed behaviour of a small horizontal axis wind turbine, *Journal of Wind Engineering and Industrial Aerodynamics*. **92**:1265-1279

APPENDIX

A1: MATLAB Code for Blade Design and Optimization

```
%lambda=tip speed ratio
lambda=input('enter the value of Tip speed ratio:\n');
%R=blade length
Rtip=input('enter blade radius:\n');
%B=no. of blades
B=input('enter number of blades:\n');
%?=pitch angle
pitch =input('enter pitch angle:\n');
pi=3.143;
Rhub=0.2*Rtip;
r=0.2;
```

```

ac=0.2;
% Initializing vairable for incrementing radius
num=10; % number of blade elements
dr=(Rtip-Rhub)/num; %Width of each blade element
r=Rtip;
x=r/Rtip;
lambdar=x*lambda;
while (r>=Rhub) %loop for incrementing blade element
%Initializing values of a and adash
old_a=0.01;
old_adash=0.01;
new_a=0.1;
new_adash=0.1;
adiff=abs(old_a-new_a);
bdiff=abs(old_adash-new_adash);
maxitr=0;
itrlimit=1;
while adiff>(0.0001*itrlimit); % Second loop for calculating a and adash
%Calculation of phi and alpha
phi=atan(2/(3*lambdar));
if phi<0
phi=1.4;
end
alpha =6;
%Cl=lift coefficient
Cl=((6*10^(-5))*alpha^4)-(0.002*alpha^3)+(0.023*alpha^2)+(0.028*alpha)+0.44;
%Cd=drag coefficient
Cd=(-1*10^(-5)*alpha^4)+(0.0005*alpha^3)-(0.007*alpha^2)+(0.033*alpha)+0.029;
Cn=Cl*cos(phi)+Cd*sin(phi);
Ct=Cl*sin(phi)-Cd*cos(phi);
%Definiing initial blade geometry
%c=Initial chord length
chord=((8*pi*r)/(B*Cl))*(1-cos(phi));
% blade twist
twist=(phi*(180/pi))-alpha-pitch;
%Definiing blade lift and drag coefficients
%sigma=solidity
sigma=(B*chord)/(2*pi*r);
%f=tip loss
f1=(2/pi)*acos(exp(-(B/2)*(1-(r/Rtip)))/((r/Rtip)*sin(phi)));
%f=f1*pi/180;
% Glauert's correction for thrust factor and calulation of new a and adash
if old_a>ac
K=(4*f1*(sin(phi))^2)/((B*chord)/(2*pi*r)*Cn);
y=(K*(1-(2*ac)));
if K<0
break
elseif y<0

```

```

break
end
new_a = (1/2)*((2+y) -((y+2)^2+4*(K*ac^2-1))^0.5);
% ct=(sigma*(1-old_a)^2*(Cl*cos(phi)+Cd*sin(phi)))/((sin(phi))^2);
else
new_a = 1/(1+(4*f1*(sin(phi))^2)/(sigma*Cn*cos(phi)));
% new_a=(0.143+sqrt(0.0203-(0.6427*(0.889-ct))))/f;
end
new_adash=1/((4*f1*cos(phi))/(sigma*Ct))-1);
%Calculating new values of adiff and bdiff
adiff=abs(new_a-old_a);
bdiff=abs(new_adash-old_adash);
old_a=(new_a+old_a)/2;
old_adash=(new_adash+old_adash)/2;
maxitr=maxitr+1;
if maxitr>10 && maxitr<165
itrlimit=maxitr;
elseif maxitr>150
break
end
end
end
%c l=chord length l
chord1=((8*pi*r)/(B*Cl))*(1-cos(phi));
if chord1<0;
chord1=0.0000001;
end
%theta=angle of twist
theta=(phi*(180/pi)-alpha)-pitch;
%sigma1=solidity
sigma1=(B*chord1)/(2*pi*r);
%Print final values of a,adash, chord and theta at a given blade element
%fprintf('the value at blade station num%f,
chord%f,new_a%f,new_adash%f,theta1%f,num,chord,new_a,new_adash,theta);
fprintf('the value at blade station x=
%f,chord1=%f,a=%f,adash=%f,theta=%f,adiff=%f\n',x,chord1,new_a,new_adash,theta,adiff);
r=r-dr;
lambdar=(r/Rtip)*lambda;
x=r/Rtip;
end

```